Surface Induced Tilt Propagation in Thin Films of Semifluorinated Liquid Crystalline Side Chain Block Copolymers

Peter Busch,*,†,‡,|| Sitaraman Krishnan,† Marvin Paik,† Gilman E. S. Toombes,§ Detlef-M. Smilgies,‡ Sol M. Gruner,*,‡,§ and Christopher K. Ober†

Department of Materials Science and Engineering, Cornell University, Bard Hall, Ithaca, New York 14853, Cornell High Energy Synchrotron Source (CHESS), Wilson Laboratory, Cornell University, Ithaca, New York 14853, and Department of Physics, Laboratory of Atomic and Solid State Physics, Cornell University, Ithaca, New York 14853

Received May 5, 2006; Revised Manuscript Received September 18, 2006

ABSTRACT: The supramolecular self-assembly within a liquid crystalline block copolymer thin film with mesogenic semifluorinated alkyl side groups was studied using both grazing incidence X-ray diffraction and small angle scattering. Previous studies employing near-edge X-ray absorption fine structure spectroscopy indicated that mesogens at the film surface are tilted relative to the surface-normal. This tilt may arise from the interplay between the low surface energy of perfluoromethyl groups and the entropic degrees of freedom of each side chain (constrained by neighboring mesogens in the smectic layer and the alkyl linker attachment to the polymer backbone). Here, we show that the mesogen tilt at the surface propagates over several smectic layers into the film interior. We propose that the high grafting density of side chains in combination with a head-to-head arrangement of side chain free ends plays a significant role in transmitting mesogen tilt from the surface to the adjacent smectic layers within the film interior. In addition to scattering from individual mesogens, we observed characteristic scattering patterns in the plane of incidence produced by the horizontal smectic layers. The amorphous polystyrene block formed vertical domains interspersed in the liquid crystalline matrix, resulting in out-of-plane Bragg rods.

Introduction

Block copolymers with liquid crystalline (LC) side chains possess two extra levels of self-assembly in addition to the assembly of blocks into periodic microdomains commonly seen in linear coil−coil diblock copolymers. In the liquid crystalline domains, the mesogenic side chains can assemble into the lamellar layers of a smectic mesophase, and in addition to this level of organization, the individual side chains are structured within each smectic lamella. Small rodlike mesogenic molecules frequently form smectic phases owing to lateral intermolecular forces. In the case of a polymer with rigid, rodlike side chains, the high grafting density of the mesogens to a flexible polymer backbone further promotes the formation of smectic phases, even in the absence of strong attractive forces between mesogens. An interesting case is that of fluoroalkyl groups which have liquid crystalline mesogenic properties. The large size of fluorine atoms in a perfluoroalkane hinders rotation around C−C bonds, making the molecule rigid.[1] Thus, despite the high dipole moment of the C−F bond, perfluorinated linear alkanes are highly nonpolar and have weak intermolecular forces due to a symmetric distribution of charges. The nonpolar nature of perfluoroalkyl groups makes them potentially useful as coatings in a variety of technological applications. Thin films of fluoropolymers have been used in microfluidics,[2] as lubricants for the protection of disk surfaces inside disk drives[3] and as anti-biofouling surfaces.[4,5]

* To whom correspondence should be addressed. E-mail: (P.B.) p.busch@fz-juelich.de; (S.M.G.) smg26@cornell.edu.

† Department of Materials Science and Engineering, Cornell University.

‡ Cornell High Energy Synchrotron Source (CHESS), Wilson Laboratory, Cornell University.

§ Department of Physics, Laboratory of Atomic and Solid State Physics, Cornell University.

|| Present address: JCNS FRMII, Lichtenbergstr. 1. TU München, 85747 Garching, Germany.

We have previously used near edge X-ray absorption fine structure spectroscopy (NEXAFS) to study the molecular structure and orientation within the top 20−30 Å of thin films of diblock copolymers with semifluorinated alkyl side chains (see a current review[6] and the references therein). These block copolymers contained a polystyrene block and a polyisoprene block to which perfluoroalkyl groups were attached through a flexible hydrocarbon spacer (Figure 1). The uniaxial orientational order parameter, determined from the change in the transitional probability of the C 1s → σ^*_{C-F} electronic transitions with the angle of polarization of the incident X-ray beam, was used to determine the average-tilt angle, $\langle\tau_{F-helix}\rangle$, of the fluoroalkyl helices relative to the surface normal.[7] It was found that $\langle\tau_{F-helix}\rangle$ decreased as the fluoroalkyl mesogen increased in length, and increased with the number of $-CH_2-$ groups in the hydrocarbon spacer.[8,9] The precise reason for the tilt of the fluorohelix is not known,[10] but probably has its origin in the interplay between the tendency of the surface to be covered by the low-energy $-CF_3$ groups (which favors homeotropic alignment) and the entropic degrees of freedom of the mesogen (which is expected to cause a tilted orientation). Self-assembled monolayers of partially fluorinated alkanes on silicon wafers showed an almost homeotropic arrangement of the fluorinated groups at the surface,[11] whereas, a LC block copolymer with $-(CH_2)_9(CF_2)_{10}F$ side chains showed a tilt angle of about 41°.[8,9] Similarly, side chains terminated with the more polar $-CF_2H$ groups, instead of the $-CF_3$ group, showed a greater tilt.[7] This observation suggests that polarity plays a role in determining the molecular organization at the surface.

While information about the molecular organization at the surface has been obtained using NEXAFS, there are few details known about the self-assembly of block copolymers with liquid crystalline side chains within thin films. Recently, Al-Hussein et al. investigated thin films of methyl methacrylate and

10.1021/ma061009+ CCC: $37.00
Published on Web 12/13/2006

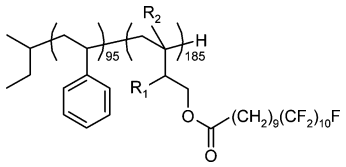

Figure 1. Structure of the liquid crystalline block copolymer with semifluorinated side chains. R_1 and R_2 can be either H or CH_3.

fluorinated acrylate based block copolymers with the combination of X-ray reflectometry and grazing incidence small-angle X-ray scattering and diffraction to probe the vertical and lateral structure of the thin films, respectively.[12] The interaction between phase separation and liquid crystallinity in determining the film microstructure was evident from their study. However, the molecular orientation and order within the smectic layers was not fully characterized and the tilt of the mesogens was not determined.

In the present study we have used 2-dimensional grazing incidence small-angle X-ray scattering (GISAXS) and diffraction (GID) to probe the self-assembly of a spin-coated film of a block copolymer consisting of a polystyrene block with an isoprene block modified with semifluorinated side groups (Figure 1). These techniques allow the investigation of both order and orientation at three different length scales of self-assembly, defined in Figure 2: D_{micro}, characterizing the microphase separation of the polystyrene domains; D_{layer}, relating to the smectic layer thickness; D_{meso}, characteristic of the intermesogen spacing within a smectic layer. In the following, we will also distinguish between the smectic layer in bulk $D_{layer,b}$ and that of the thin film, $D_{layer,f}$. We found that the mesogenic groups in these block copolymer thin films showed a tilt throughout the thickness of the film, in contrast to bulk samples of these polymers which are known to form smectic B and smectic A mesophases.[13] Because the angle of tilt determined by GISAXS was similar to the tilt of the mesogens at the surface (determined by NEXAFS), we propose that the film surface induces a tilt of the mesogens which propagates through several smectic layers of the film.

Experimental Section

Materials. Side chain liquid crystalline block copolymers were prepared by polymer analogous reaction on polystyrene-*block*-polyisoprene (PS-*b*-PI) synthesized by anionic polymerization, as reported previously.[14] Styrene was polymerized in tetrahydrofuran at −78 °C using *sec*-butyllithium as the initiator. An aliquot of sample was withdrawn for molecular weight determination. The polystyryllithium macroinitiator was then used to initiate polymerization of isoprene. The living chain ends were finally terminated with methanol. The reaction conditions used resulted in predominantly pendent vinyl groups (1,2- and 3,4-addition) in the isoprene block. Hydroxyl groups were introduced in the isoprene block by the hydroboration/oxidation reaction using 9-borabicyclononane (9-BBN) and hydrogen peroxide, which were reacted with the semifluorinated acid chloride, $F(CF_2)_{10}(CH_2)_9COCl$, to obtain a block copolymer with semifluorinated side chains. Using gel permeation chromatography (Waters Styragel HT columns and Waters 490 UV detector) the molecular weight of the PS block was found to be 10 000 g/mol with a polydispersity index of 1.04. The molecular-weight of the PI block, determined by ^1H NMR (Varian Gemini 300 MHz spectrometer, $CDCl_3$ solvent) from the ratio of the aromatic protons and all the protons in the block copolymer, was 12 500 g/mol. The polydispersity index of the PS-*b*-PI polymer, determined by GPC, was 1.08. The degrees of polymerization of the PS and PI blocks were about 95 and 185, respectively. The amount of 1,4-addition was estimated to be around 12%. The esterification of the hydroxyl groups with the semifluorinated acid chloride was confirmed using IR spectroscopy (Mattson 2020 Galaxy Series FTIR spectrometer) by the disappearance of the O−H stretching vibrations at 3334 cm^{-1} of the hydroxylated PS-*b*-PI precursor, and appearance of ester C═O stretching vibrations at 1737 cm^{-1} and C−F band between 1000 cm^{-1} and 1400 cm^{-1}. As expected, the fluorinated block copolymer was found to be liquid crystalline using DSC (TA Instruments Q1000 calorimeter). Two distinct first-order transitions were observed at 98 °C and 113 °C, and based on previous studies, attributed to smectic-B to smectic-A, and smectic-A to isotropic transitions, respectively. From the monomer molecular weight of 758.45 g/mol, the weight fraction of the fluorinated block in the block copolymer was calculated to be 0.93. Using Kier-Hall molecular connectivity indices,[15] the fluorinated block is estimated to have a density of about 1.64 g/cm^3. Thus, the volume fraction of the fluorinated block is expected to be about 0.89. The PS domains are immersed in the smectic phase with a spacing of $D_{micro} = 2\pi/q = 250$ Å and a smectic layer distance $D_{layer,b}$ of 51.6 Å as determined by transmission SAXS on a bulk sample at G1 station at the Cornell High Energy Synchrotron Source (CHESS).

Thin Film Preparation. Thin films of the block copolymer were prepared by spin-coating a 1% (w/v) solution of the polymer in α,α,α-trifluorotoluene (TFT) onto a silicon wafer using a Cee model 100CB spin-coater at 3000 rpm for 30 s. The film was annealed in a vacuum oven at 150 °C for 12 h, after which the heating was stopped and the samples slowly cooled to room temperature. The film thickness was about 700 Å as determined by AFM from the height at a scratch near to the center of the sample. A Dimension 3100 microscope together with a Nanoscope IV controller from Digital Instruments and Olympus cantilevers with a resonance frequency of about 230 kHz were used.

GISAXS and GID. GISAXS and GID images were obtained at G1 station at the Cornell High Energy Synchrotron Source (CHESS) at a wavelength $\lambda = 1.23$ Å. The details of the experimental setup have been described elsewhere[16] and will be outlined only briefly. The beam was collimated to a height of 100 μm and a width of 300 μm by three sets of slits. Two beam stops were used in front of the detector: (i) a blade to block the direct beam and (ii) a tantalum rod 1.25 mm wide to block the intense specular reflected beam. The experimental setup as well as the geometrical notations used throughout this manuscript are defined in Figure 3.

While there are different conventions to define an appropriate coordinate system in reciprocal space for a scattering or diffraction setup under grazing incidence, we have defined the incoming beam (wave vector $\boldsymbol{k}_i$) to lie along the *x*-axis. Defining the position of the direct beam on the detector to be (Y_b, Z_b), radiation scattered through an angle 2θ (wave-vector $\boldsymbol{k}_f = \boldsymbol{q} + \boldsymbol{k}_i$) is then detected at ($Y_b + L_{sd} \tan 2\theta \cos \phi_d$, $Z_b + L_{sd} \tan 2\phi \sin \phi_d$) where ϕ_d is the azimuthal angle and L_{sd} the distance between sample and detector. The sample was rotated with respect to the incoming beam about the *y*-axis to adjust the incident angle α_i. The scattering vector $\mathbf{q}$, can be described by the parallel ($q_{||} = |\boldsymbol{q}| \cos \phi_d$) and perpendicular ($q_\perp = |\boldsymbol{q}| \sin \phi_d$) components of the equal-area projection of the Ewald sphere. We defined the angle between $\boldsymbol{q}$ and the sample plane to be ϕ, which is related to ϕ_d and θ by the expression

$$\sin \phi = \sin \phi_d \cos \alpha_i \cos \theta + \sin \alpha_i \sin \theta. \quad (1)$$

For the small sample tilt used here, the approximations $\phi = \phi_d$, $q_{||} = q_y$ and $q_\perp = q_z$ are valid in the small angle regime.

Images of the scattered intensity were recorded with a fiber-optically coupled CCD camera (Quantum 1 by ADSC, Poway, CA).[17] The images were corrected for background, intensity and distortion.[18]

Results

Figure 4a shows the 2-dimensional GISAXS map of the liquid crystalline side chain block copolymer at $\alpha_i = 0.17°$. The most pronounced feature is the strong signal from the smectic layers at $q_z \approx 0.15$ Å^{-1}. The intensity is mainly concentrated around

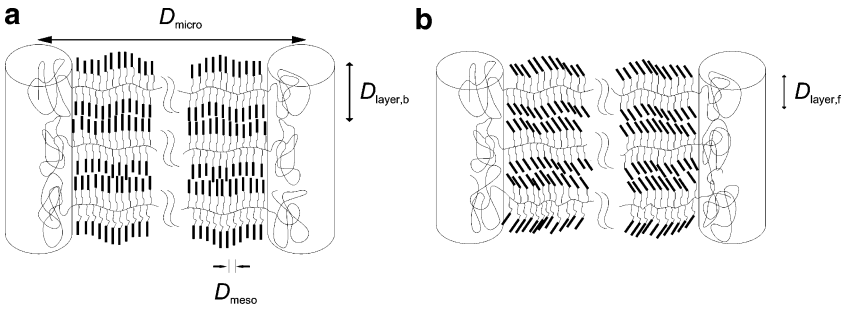

Figure 2. Model of a semifluorinated, liquid crystalline side chain block copolymer. The columns at the extreme left and right represent the microphase separated polystyrene microdomains and the short, bold bars are fluorinated side chains. Part a shows a structure with untilted fluorinated side chains while part b shows one with tilted side chains, as has been observed for thin films on the surface in this paper.

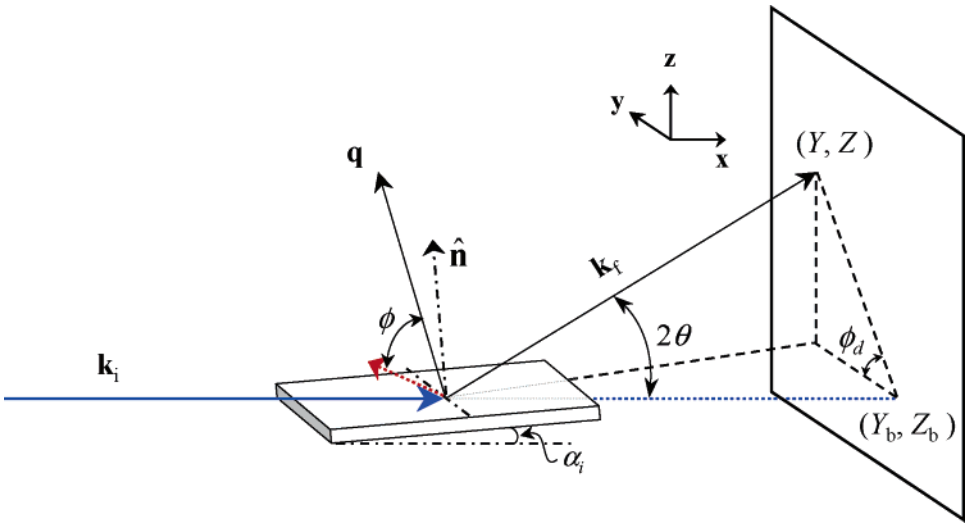

Figure 3. Scattering geometry used for the GISAXS and the GID experiments. The incident beam is directed along the *x*-axis while the sample is tilted up from horizontal by a shallow angle, α_i, in the *x*-*z* plane. The flat area detector lies parallel to the *y*-*z* plane a distance L_{SD} from the sample. The position where the incident beam would strike the detector (without a sample) is defined as (Y_b, Z_b) and we consider X-rays scattered to a point (*Y*, *Z*) on the detector. The Bragg scattering angle, 2θ is defined in the conventional way while we define ϕ_d to be the angle from the *y*-axes. $\hat{\boldsymbol{n}}$ is the sample surface normal and $\boldsymbol{q} = \boldsymbol{k}_f - \boldsymbol{k}_i$ the scattering vector which includes an angle ϕ with its projection onto the surface, as indicated by the red dotted arrow to the left.

$q_{||} = 0$ Å^{-1} and confined within a tilt distribution of the smectic layer normal $\Delta\tau_{sm}$ of $\Delta\tau_{sm} = \pm 2.5°$, as determined from the full width at half-maximum (fwhm) of a radial slice centered around the specular reflected beam (Figure 4b). Thus, the smectic layers were mainly oriented parallel to the film surface. To determine the thickness of the smectic layers, it is necessary to consider both the refraction of the incident beam when it enters and leaves the film as well as reflection from the substrate. The corrected momentum transfers measured at the detector are[19]

$$q_z(\alpha_i) = k_0\left(\sin\alpha_i + \sqrt{\sin^2\alpha_{cP} + \left[\frac{n\lambda}{D_{layer,f}} \mp \sqrt{\sin^2\alpha_i - \sin^2\alpha_{cP}}\right]^2}\right), \quad (2)$$

where $k_0 = 2\pi/\lambda$, α_{cP} is the average critical angle of the polymer film and *n* an integer. α_{cP} is related to the average density of the film, but because the density of the liquid crystalline block is highly dependent on the preparation conditions,[20] this value cannot be calculated in the classical way as for coil−coil block copolymers.[21,22] We thus conducted measurements at several incident angles and a fit of eq 2 with $n = 1$ and $\lambda = 1.231$ Å resulted in $D_{layer,f} = (44.0 \pm 0.2)$ Å and $\alpha_{cP} = (0.167 \pm 0.002)°$. The smectic layer thickness in the bulk, determined from transmission X-ray scattering, was $D_{layer,b} = 51.6$ Å. Thus, within the thin film the smectic layer distance is about 15% smaller than the bulk value, suggesting a change in mesogen packing such as a tilt of the mesogens.

To study the orientation and in-plane order of the mesogens we performed complementary GID experiments. Figure 5 shows the 2-dimensional GID map of the liquid crystalline side chain block copolymer at $\alpha_i = 0.17°$. Because of the high diffraction angles, an asymmetric setup was used, in which the specular reflected beam is located at the lower right of the detector. Correlations between the mesogens resulted in a diffraction pattern in the form of a nearly circular arc that extended from $(q_{||}, q_\perp) = (-1.29, 0.04)$ Å^{-1}. This arc showed an intensity maximum at $(q_{||}, q_\perp) \approx (-1.1, 0.75)$ Å^{-1} indicating a tilt of the mesogens. The Fresnel transmission function enhances the intensity at $q_\perp = 0.04$ Å^{-1}, while below that value the intensity is suppressed.[21,22]

To quantify the in-plane ordering of the mesogens we examined the radial dependence of scattering intensity, $I(q)$, for scattering vectors $\boldsymbol{q}$ at an angle of $0° < \phi_d < 5°$. The in-plane scattering is well-described by a Lorentzian (inset of Figure 5), from which $D_{meso} = 2\pi/q = 4.9$ Å and a correlation length of $\xi = 2/\Delta q = 15$ Å could be estimated, as determined by the fwhm. The correlation length is comparable to that of the higher ordered smectic B phase in bulk for this particular sample system and larger than the typical value found for liquid like smectic A phase without bond-orientational order.[14] Thus, the mesogens

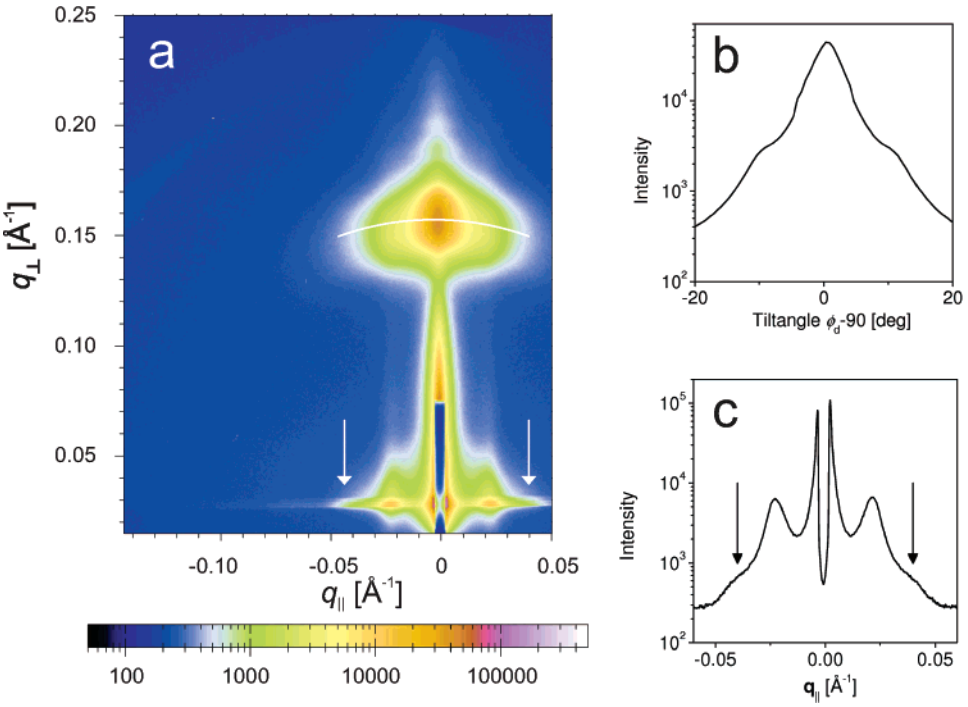

Figure 4. (a) 2-Dimensional GISAXS map at $\alpha_i = 0.17°$. The strong signal at ($q_{||} = 0$ Å $^{-1}$, $q_\perp = 0.15$ Å^{-1}) arises from the smectic layers oriented parallel to the film plane. The circular spread indicates a narrow distribution of the layer normal. The PS-domains give rise to straight Bragg rods at $|q_{||}^*| = 0.023$ Å^{-1}. (b) Radial slice through the first-order smectic layer Bragg reflection as indicated by the white arc in part a. The fwhm of the smectic layer distribution is ± 2.5°. In addition the PS domain structure is mirrored in the shoulders of the smectic peak. (c) Horizontal slice ($q_\perp = 0.03$ Å^{-1}) revealing ordering within the plane of the sample. The white arrows in (a) and the black arrows in (c) indicate a weak shoulder at $3^{1/2}|q_{||}^*|$.

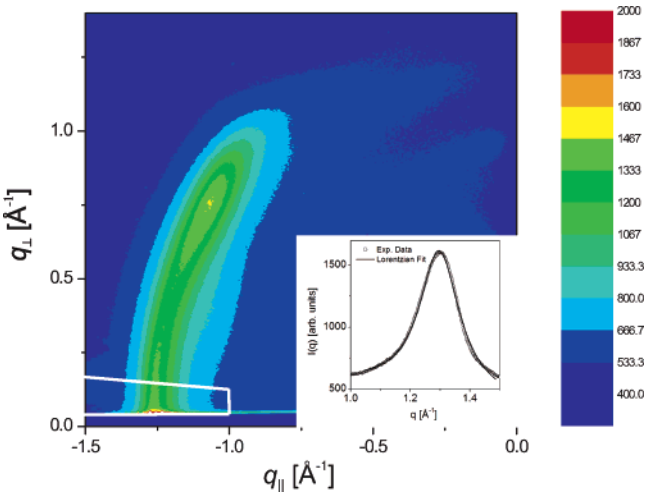

Figure 5. 2-dimensional GID-map at $\alpha_i = 0.17°$. Note that the intensity scale for this map is linear. Mesogen−mesogen correlations give rise to the broad scattering arc of radius $|q| \approx (1.28 \pm 0.05)$ Å^{-1} that extends from horizontal to an angle of $\phi_d \approx 45°$. For each narrow sector, defined as intensity along a line of constant ϕ_d (see Figure 3), scattering intensity is well described by a Lorentzian sitting on a linear background ($I(q) = c_0 + c_1 q + I_0/[q^2(1 + ((q - q_o)/q_w)^2)]$) as shown in the inset for the sector $0° < \phi_d < 5°$ indicated by the white lines.

are locally packed with substantial bond-orientational order which decays over a length scale of about three times the mesogen spacing.

The orientation of the mesogens uniquely determines the angular dependence of scattering intensity. If the direction of mesogen tilt has a unique projection into the plane (e.g. toward the nearest neighbor S_I or next-nearest neighbor S_F) the diffraction pattern should show a characteristic set of two or three distinct spots. These ordered phases have been observed for amphiphilic molecules in Langmuir monolayers where the mesogens are free to pack in a well-defined, dense lattice.[21,23,24] This well-defined packing is less likely for mesogens tethered with a high grafting density to the polymer backbone. Indeed, the observed scattering exhibits a single broad arc indicating that the mesogen tilt director is less well correlated with the direction of neighboring mesogens.

A commonly applied description of disordered mesogens is that of Leadbetter and Norris, described in the Appendix.[25] In this approach, the sample is approximated by an ensemble of individual grains (each with a unique tilt director, ***n***) which diffracts at a distinct angle. Summing the scattering from all the grains yields a broad arc which reflects the distribution of tilt directors within the sample. Although we have applied this model to our data, it overestimates the distribution of tilt angles because mesogens are treated as infinitely long cylinders. To correct for the finite mesogen length, we have introduced a mesogen form factor to the model of Leadbetter and Norris in a similar fashion as in the work of Als-Nielsen and Kjaer[23,26] describing simple ordered smectic structures.

Figure 6a shows the dependence of the integrated scattering intensity, $I(\phi) = \int I(\phi, q)q^2\, dq$, on angle, ϕ. The tilt of the mesogens can be determined by fitting the experimental data to a structural model (for details see the Appendix). We considered three models of the mesogen, the first being the infinite rod model from Leadbetter and Norris[25] and two other models where different approximations about the mesogen form factor were made. In the second model the fluorinated (length $L_F = 14$ Å)[27] and hydrogenated (length $L_H = 13$ Å)[27] segments of the mesogen are assumed to form a single rigid cylinder of total length $L = L_F + L_H$ as proposed by Russell et al.[28] The third model addresses the possibility that the hydrogenated segment is more flexible than the fluorinated mesogen, and therefore less straight and ordered.[11] In this case the fluorinated segment dominates the diffraction because of its high electron

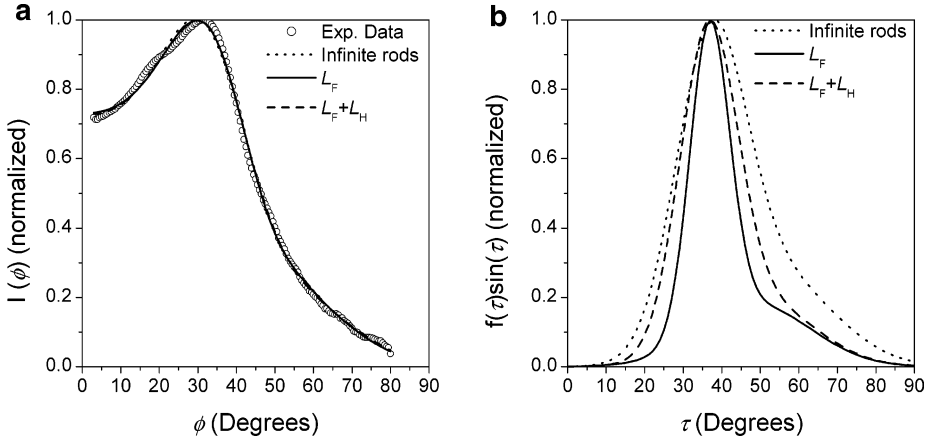

Figure 6. (a) Integrated scattering intensity in dependence on ϕ (circles) and fits from the three models considered in text. b) Tilt distributions $f(\tau)$ sin τ vs τ for the models considered in a). Infinite rod model: $\tau = 42.5°$, $\Delta\tau_{fwhm} = \pm 12°$, (dotted line). Tilt of the fluorinated segment only: $\tau = 41.2°$, $\Delta\tau_{fwhm} = \pm 6.7°$, (full line). Fluorinated+Hydrogenated segment model: $\tau = 40.3°$, $\Delta\tau_{fwhm} = \pm 9.6°$, (dashed line). Note that tilt angles obtained from the intensity distributions in part b are significantly larger than the angle where the radial intensity distribution in part a has its maximum ($\sim 29.5°$).

density (77% of the electrons) and the mesogen can be approximated by a cylinder of length $L = L_F$. By considering these two scenarios, we ensure that our analysis accommodates the actual hydrogenated segment conformation.

As seen in Figure 6a, the Leadbetter model ($L = \infty$), the full mesogen model ($L = L_F + L_H = 25$ Å) and the fluorinated segment only model ($L = L_F = 14$ Å) all fit the data well and yield a mean tilt angle in the range of $\tau = 40.3$ to $42.5°$. It is thus not possible to distinguish between the three models from the experimental data. The significant difference between the three models is reflected in the estimated distribution of tilt angles. As expected, the Leadbetter model overestimates the tilt distribution with $\Delta\tau_{fwhm} = \pm 12°$, obtained from the full width at half-maximum. Depending on how disordered or straight the hydrogenated segment is, the true distribution can be better approximated by introducing an expression for the form factor, as shown in the Appendix. This results in a lower value of $\Delta\tau_{fwhm} = \pm 6.7°$ ($L = L_F$) and $\Delta\tau_{fwhm} = \pm 9.6°$ ($L = L_F + L_H$). Although the smectic layers were found to have a mosaicity $\Delta\tau_{sm} = \pm 2.5°$, this contribution to the mesogen tilt is small ($\Delta\tau_{corr} = (\Delta\tau^2 - \Delta\tau_{sm}^2)^{1/2}$ of $\pm 11.7°$, $\pm 6.2°$ and $\pm 9.3°$, respectively).

The tilt distribution obtained by fitting the experimental data was found to be centered near 41°, which is in very good agreement with the value of 41° determined by NEXAFS spectroscopy of the film surface.[8] It is important to note that the observed diffraction pattern stems from the entire film and cannot be explained by a tilt of the mesogens in a near surface region only. If the mesogen tilt diminished noticeably with further distance from the surface of the film, the GID pattern would be concentrated at $\phi = 0°$ at higher incident angles, i.e., larger X-ray penetration depth. Additionally, the scattering from the smectic layers would show broadened peaks in q_z as the smectic layer thickness would change throughout the film. Furthermore, measurements below α_{cP} did not show any significant diffraction, indicating that the scattering power of the top layer is not strong enough to give rise to the observed scattering pattern. We have conducted measurements at incident angles up to 0.22° and found no significant differences. Thus, the tilt observed by our GID experiments appears to be a surface-induced effect and must extend quite far into the film.

The effect of steric constraints on the densely grafted mesogens may explain both the relatively large distribution of mesogen tilts as well as the propagation of tilt through the layers. The mesogens are grafted to the backbone every two carbon−carbon bonds—a distance of 2.5 Å. Even if one considers the 12% 1,4-addition the distance between the grafting sites can be estimated to be around 3 Å. The van der Waals diameter of the fluorinated rod segment of the mesogen is 6 Å, which is about the same value.[10,11] This dense grafting of mesogens onto the backbone severely constrains both the backbone and mesogens. Even for the S_B phase observed in bulk for this system, along a single backbone adjacent mesogens are likely to alternate between upper and lower smectic layers so as to alleviate some of this packing stress (Figure 2a). The requirement that each mesogen is connected to a backbone frustrates the packing of mesogens onto a regular lattice with a unique tilt orientation. Instead, mesogens are likely to tilt toward the backbone to which they are grafted resulting in a comparatively broad distribution of mesogen tilt angles. The net mesogen tilt at the surface increases the area per mesogen and stress on the backbone. The alternating arrangement of mesogens (Figure 2) automatically couples the tilt angle for any pair of upper and lower smectic layers. If the fluorinated chain ends of neighboring lower and upper layers pack in a head-to-head conformation, tilt will then be transferred from one smectic layer pair to the next. In combination, these two interactions are a plausible mechanism by which the tilt of mesogens at the surface could be transferred to the underlying smectic layers.

Finally we consider the structure of the PS-domains that are immersed in the highly ordered structure of the LC-block. The ordering of PS domains within the plane of the film gives rise to the vertical Bragg rods at $|q_{||}^*| = 0.023$ Å^{-1} seen in Figure 4a, where $q_{||}^*$ is the position of the first order Bragg rod. The Bragg rods are straight and their intensity smoothly decays with increasing $q_\perp$, implying that the structure of PS domains is relatively uniform along the direction of the film normal. Along $q_{||}$, the Bragg rods are fairly broad ($\Delta q_{||} = 0.008$ Å^{-1}), but an additional weak shoulder can be seen at $|q_{||}| = (3^{1/2})|q_{||}^*|$ as indicated by the black arrows in Figure 4c.

Although the shoulder at $(3^{1/2})q_{||}^*$ suggests that the polystyrene domains are arranged in a hexagonal lattice, a unique determination of the block copolymer morphology is challenging without additional, higher-order peaks. Because of the low volume fraction of polystyrene, the PS domains are most likely to be spheres or cylinders. The GISAXS signature of cylinders lying parallel to the film surface has been reported in the literature,[29] and can be clearly excluded in our case. Also, the

scattering patterns reported for spherical polystyrene domains (e.g., Xu et al.[30]) are quite different from the rather straight Bragg rods we observe. In contrast, the GISAXS pattern is entirely consistent with cylindrical domains of polystyrene standing normal to the surface. Indeed, the observed diffraction is comparable to that from cylindrical block copolymer films prepared by spin-coating.[31] This morphology also matches studies of the surface topography with AFM (data not shown) showing dots with a well-defined nearest neighbor distance but only short-range order. Although the AFM data cannot confirm that individual columns of polystyrene are uniform from substrate to surface, standing PS cylinders are most consistent with the experimental data.

The average distance between PS-domains, $D_{\text{micro}} = 2\pi/|q_{||}^*| = 272$ Å, is about 8% larger than the value measured in bulk. A plausible explanation would be that in the case of liquid crystalline side chain polymers, the polymer backbone to which the mesogens are attached is expected to be in a more relaxed conformation when the mesogens are oriented normal to the polymer backbone. Tilt increases the effective area per mesogen along the backbone forcing the latter to have a more extended conformation. This extended conformation of the main chain of the LC block is reflected in the larger distance between the polystyrene domains in the thin film compared to that in the bulk. Interestingly, the increase in area between polystyrene domains (16%) is very similar to the decrease of the smectic layer thickness (15%). Finally, the in-plane correlation length ($2/\Delta q_{||} = 730$ Å) is less than three times the distance between PS domains, suggesting that the highly ordered internal structure of the LC-block dominates the morphology and prevents the packing of PS-domains into a well-defined lattice. Instead, the morphology might be better described by PS-domains immersed with only short-range order in the surrounding smectic domain.

Conclusion

The self-organization of the liquid crystalline side chain block copolymers discussed in this manuscript is dominated by the strong tendency of the fluorinated end groups to segregate to the film surface to form a low energy surface. The side chains of the liquid crystalline block self-organize into smectic layers which are oriented parallel to the film surface. Inside the layers the side chains are tilted with respect to the smectic layer normal with a broad tilt distribution, which is different from the bulk morphology for this class of materials. The observed tilt is in very good agreement with the tilt in the top layer at the surface, which has been observed by NEXAFS experiments.[8] The tilt propagates over several smectic layers into the film. We attribute this tilt propagation to a combined effect of the high grafting density of mesogens to the polymer backbone and the head-to-head interaction of chain ends of adjacent smectic layers. In addition to scattering from individual mesogens, we observed characteristic scattering patterns in the plane of incidence produced by the horizontal smectic layers. The amorphous polystyrene block formed vertical domains interspersed in the liquid crystalline matrix, resulting in out-of-plane Bragg rods.

Appendix

Mesogen−mesogen scattering from liquid crystal structures has traditionally been interpreted either in the context of highly ordered structures[32] or highly disordered structures.[25,33]

Approaches for highly ordered structures treat the mesogens as rods with a unique tilt angle and orientation packed on a perfect 2-D crystal. The shape of the lattice and the orientation of the mesogen then uniquely predict the location of three sharp diffraction spots, which can be degenerate or not, depending on the tilt angles τ and ψ.[21,32] Although Als-Nielsen and Kjaer have considered the mesogen form factor,[26] the effect of a distribution of tilt directions has not been considered. This is a reasonable approach for well ordered systems like fatty acids on the air−water interface[32] or low molecular weight liquid crystals.[34] Conversely, models for poorly ordered mesogens approximate the mesogens as infinitely long rods with liquidlike ordering and a distribution of tilts. The broad distribution of tilt directions produces a broad arc of scattering and the tilt distribution is related to the scattering arc by an integral expression.[25]

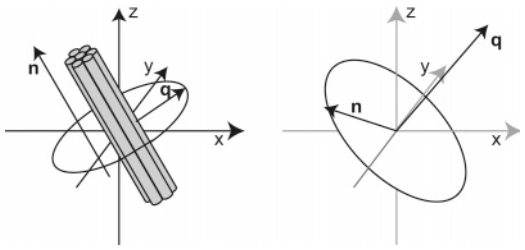

Figure 7. In Leadbetter's model,[25] the mesogens are long, thin rods which are locally well-aligned along a local mesogen director $\boldsymbol{n}$. For each bundle of rods, scattering is concentrated at right angles to the bundle. Thus, scattering vectors that lie on the ring $\boldsymbol{q}\cdot\boldsymbol{n} = 0$ show the brightest scattering. Although the mesogens have strong orientational order locally, across the sample the director assumes a distribution of values. The experimentally observed scattering at $\boldsymbol{q}$ will be dominated by mesogens directed at right angles to $\boldsymbol{q}$. The intensity at $\boldsymbol{q}$ is a sum over all the mesogens with directors, $\boldsymbol{n}$ lying on the ring $\boldsymbol{q}\cdot\boldsymbol{n} = 0$.

The mesogens and scattering data considered in this paper are intermediate between these two extremes. Thus, the approach considered in this manuscript will focus on the combination of the two approaches. We will consider first the infinite rod model of Leadbetter and Norris and then include expressions for the mesogen form factor.

Liquid-Like Model of "Long" Mesogens. Leadbetter and Norris first developed a model for interpreting the broad scattering arcs produced by tilted mesogens.[25] These authors used a relatively simple approach for the mesogen form factor by treating the mesogens as long cylindrical rodlike particles with length L and diameter D, where $L \gg D$. Locally the mesogens are well correlated and oriented with respect to a local mesogen director, $\boldsymbol{n}$, as shown in Figure 7. Scattering from this single "grain" occurs only for $\boldsymbol{q}$ at right angles to the rods ($\boldsymbol{n}$) for a single magnitude of $|\boldsymbol{q}| = q_0$ corresponding to the mesogen-mesogen distance. In this model, the broad arc of scattering arises because in different parts of the sample the local mesogen director, $\boldsymbol{n}$, assumes different orientations. Reversing our perspective, for a given scattering vector $\boldsymbol{q} = q(\cos\phi\hat{\boldsymbol{y}} + \sin\phi\hat{\boldsymbol{z}})$, scattering can only come from grains with rods at right angles to $\boldsymbol{q}$, as shown in Figure 7. Thus, the scattering intensity, $I(\phi)$ at an angle ϕ is a sum of contributions from mesogens with tilts in the range of

$$\phi \le \tau \le \frac{\pi}{2}$$

We now obtain an expression for $I(\phi)$ in terms of the distribution function for the mesogen tilts $f(\tau)$. Scattering with wave vector $\boldsymbol{q} = q(\cos\phi\hat{\boldsymbol{x}} + \sin\phi\hat{\boldsymbol{z}})$ from a single "grain" with director $\boldsymbol{n}$ is given by

$$I(\boldsymbol{q}) = I_0\frac{V^{2/3}}{2\pi q_0}\delta((\boldsymbol{q}\cdot\boldsymbol{n})V^{1/3})\delta((|\boldsymbol{q}| - q_0)V^{1/3}) \qquad (3)$$

where I_0 is the total scattered intensity, V is the volume and q_0 is the radius of the diffuse ring in reciprocal space ($q_0 \approx 2\pi/D_{meso}$). The total scattering, $I(\phi, q)$ is obtained by integrating over all possible grain directors $\boldsymbol{n} = \sin\tau\cos\chi\hat{\boldsymbol{x}} + \sin\tau\sin\chi\hat{\boldsymbol{y}} + \cos\tau\,\hat{\boldsymbol{z}}$, weighted by the fraction of grains with that orientation, $f(\tau)\sin\tau\,d\tau\,d\chi$,

$$I(\phi, q) = \int_{\tau=0}^{\tau=(\pi/2)} \int_{\chi=0}^{\chi=2\pi} I_0 \frac{V^{2/3}}{2\pi q_0} \delta(qV^{1/3}(\cos\phi\sin\tau\cos\chi + \sin\phi\cos\tau)) \times \delta((q - q_0)V^{1/3}) f(\tau)\sin\tau\,d\tau\,d\chi, \quad (4)$$

where χ is the angle of the grain director projected onto the $x - y$ plane. Since scattering only occurs for $q = q_0$, we integrate across the peak to give the pure angular dependence,

$$I(\phi) = \int_{q=0}^{q=\infty} I(\phi, q) q^2\,dq \quad (5a)$$

$$I(\phi) = \int_{\tau=\phi}^{\tau=(\pi/2)} \frac{I_0 f(\tau)\sec\phi\tan\tau\,d\tau}{2\pi\sqrt{\tan^2\tau - \tan^2\phi}} \quad (5b)$$

Equation 5 permits direct calculation of the scattering pattern that results from a given distribution of mesogen tilt angles, $f(\tau)$. In practice, of course, the relationship is used in reverse to infer the mesogen tilt distribution from an experimentally measured $I(\phi)$. Direct numeric inversion of the integral is somewhat difficult. A more robust practice is to assume an analytic form for $f(\tau)$ and determine coefficients by nonlinear least squares. Figure 6b shows the result of such a fit to the experimental measurements. The tilt distribution has a mean value of $\tau_{COM} = 42.5°$ and distribution of $\Delta\tau_{fwhm} = \pm 12°$.

Although there are several approximations in the Leadbetter-Norris model, the most restrictive is that $L \gg D$. For mesogens of finite length the angular spread of scattering has a natural fwhm of approximately D/L which increases the apparent tilt distribution determined from eq 5. The mesogens we studied have a diameter of $D \approx 5.6$ Å[28,35] and an extended length of the fluorinated and hydrogenated mesogen segments of $L_F = 14$ Å and $L_H = 13$ Å respectively[27] which contributes 10 to 20° to the width of $I(\phi)$.

Introducing a Form Factor. The most direct way to improve the Leadbetter and Norris model is to improve the expression of the mesogen form factor. Fortuitously, this is simplest for a 2-D perfect crystal so the re-formulation simultaneously refines models of well-ordered mesogens.[32] In this section we develop an expression for $I(\phi)$ for a 2-D crystal with known lattice and mesogen form factor. The multitude of conformations within the smectic C phase can then be approximated by averaging over an ensemble of crystallites. The effect of a distribution of mesogen tilt angles is incorporated in the same manner.

The scattering observed at a wave vector $\boldsymbol{q}$ from a 2-D crystal in x−y plane is given by

$$I(\boldsymbol{q}) = I_0 V |F(\boldsymbol{q})|^2 \sum_j \delta((\boldsymbol{q} - \boldsymbol{q}^j)\cdot\hat{\boldsymbol{x}}V^{1/3})\delta((\boldsymbol{q} - \boldsymbol{q}^j)\cdot\hat{\boldsymbol{y}}V^{1/3}) \quad (6)$$

where $F(\boldsymbol{q})$ is the Fourier transform of the mesogen and $\boldsymbol{q}^j$ are reciprocal lattice vectors. For roughly cylindrical mesogens packed in a quasi-hexagonal lattice, the innermost diffraction ring has six reciprocal lattice vectors. Within a sample there are many grains and averaging over them is equivalent to averaging $\boldsymbol{q} = q\cos\phi\cos\chi\hat{\boldsymbol{x}} + q\cos\phi\sin\chi\hat{\boldsymbol{y}} + q\sin\phi\hat{\boldsymbol{z}}$ about the z-axis ($0 \le \chi \le 2\pi$). Thus,

$$I(\phi, q) = I_0 V \int_{\chi=0}^{\chi=2\pi} \frac{d\chi}{2\pi} |F([q\cos\phi\cos\chi, q\cos\phi\sin\chi, q\sin\phi])|^2 \times \sum_j \delta((q\cos\phi\cos\chi - \boldsymbol{q}^j\cdot\hat{\boldsymbol{x}})V^{1/3})\delta((q\cos\phi\sin\chi - \boldsymbol{q}^j\cdot\hat{\boldsymbol{y}})V^{1/3}) \quad (7)$$

As only the angular dependence of scattering is of interest we perform again the integration of eq 5a to obtain

$$I(\phi) = \frac{I_0}{\pi}\sum_j \frac{V^{1/3}|\boldsymbol{q}^j|}{\cos^3\phi} |F([q_x^j, q_y^j, |\boldsymbol{q}^j|\tan\phi])|^2 \quad (8)$$

Equation 8 permits the rapid evaluation of $I(\phi)$ provided the Fourier transform $F(\boldsymbol{q})$ of the mesogen and the six innermost Bragg peaks of the 2-D lattice, $\boldsymbol{q}^j$, are known.

Analytical Expression for Form Factor. To apply eq 8, we need to specify both the mesogen form factor and the 2-D lattice. In this section, we consider the form factor and packing of cylindrical mesogens. Figure 8 illustrates our cylindrical model for a semifluorinated alkane. The mesogen is divided into two segments, and the density in each segment is approximated by a product of an axial and a radial term. Our approach is similar to that from Als-Nielsen and Kjaer who treated the mesogens as perfect cylinders.[26] In our model we will introduce expressions which account for the roundness of the ends of the mesogens as shown in Figure 8.

We first consider the form factor of the mesogen. For the fluorinated segment the electron density is modeled as

$$\rho_F(r, l) = \frac{N_F}{L_F} \times \frac{\operatorname{erf}\left(\frac{l + \frac{L_F}{2}}{\sqrt{2}\sigma_l}\right) - \operatorname{erf}\left(\frac{l - \frac{L_F}{2}}{\sqrt{2}\sigma_l}\right)}{2} \times \frac{r^2}{4\pi\sigma_{Fr}^4} \times \exp\left(\frac{-r^2}{2\sigma_{Fr}^2}\right) \quad (9)$$

where l is the distance along the fluorinated segment axis (from the middle of the segment), r the radius out from the mesogen, $N_F = 249$ the number of electrons in the segment, $L_F = 14$ Å the length of the segment, $\sigma_l = 1$ Å the sharpness of each "end" of the segment (approximately 1 bond length) and $\sqrt{2}\sigma_{Fr} = 0.85$ Å the radius from the segment axis at which the electron density is maximum (to model the grouping of fluorine atoms in a helix around the carbon backbone in Teflon[36]).

Similarly, the hydrogenated segment electron density profile is modeled as

$$\rho_H(r, l) = \frac{N_H}{L_H} \times \frac{\operatorname{erf}\left(\frac{l + \frac{L_H}{2}}{\sqrt{2}\sigma_l}\right) - \operatorname{erf}\left(\frac{l - \frac{L_H}{2}}{\sqrt{2}\sigma_l}\right)}{2} \times \frac{\exp\left(\frac{-r^2}{2\sigma_{Hr}^2}\right)}{2\pi\sigma_{Hr}^2} \quad (10)$$

where l is the distance along the hydrogenated segment (from the middle of the segment), r the radius out from the segment axis, $N_H = 72$ the number of electrons in the hydrogenated segment, and $L_H = 13$ Å the segment length and $\sigma_{Hr} = 0.8$ Å approximates the "radius" out to which electron density extends from the zigzag of the carbon backbone. For both $\rho_F(r, l)$ and $\rho_H(r, l)$ the first term defines the length while the second

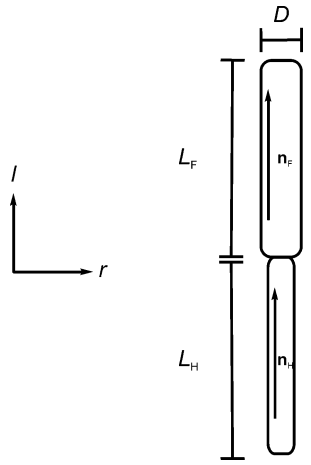

Figure 8. Illustration of a cylindrical model of a semifluorinated alkane. The model consists of two segments. The fluorinated segment has a director, $\boldsymbol{n}_F$, diameter $D = 5.6$ Å and length $L_F = 14$ Å. The hydrogenated segment has a director $\boldsymbol{n}_H$ and length $L_H = 13$ Å.

confines the electrons to close to the mesogen axis. Other expressions for the density that meet these criteria should lead to similar results.

To compute the Fourier transform of the density, we require the components of a wave vector $\boldsymbol{q}$ along the axis and radius of a segment. These are given by

$$q_l = \boldsymbol{q}\cdot\boldsymbol{n} \tag{11}$$

$$q_r = \sqrt{|\boldsymbol{q}|^2 - q_l^2} = \sqrt{|\boldsymbol{q}|^2 - (\boldsymbol{q}\cdot\boldsymbol{n})^2} \tag{12}$$

where $\boldsymbol{n}$ is the segment director. Thus, the Fourier transform of the two segments are

$$F_F(\boldsymbol{q}) = N_F \times \mathrm{sinc}\left(\frac{(\boldsymbol{q}\cdot\boldsymbol{n}_F)L}{2}\right) \times \exp\left(\frac{-\sigma_l^2(\boldsymbol{q}\cdot\boldsymbol{n}_F)^2}{2}\right) \times \left(1 - \frac{(|\boldsymbol{q}|^2 - (\boldsymbol{q}\cdot\boldsymbol{n}_F)^2)\sigma_{Fr}^2}{2}\right) \times \exp\left(\frac{-\sigma_{Fr}^2(|\boldsymbol{q}|^2 - (\boldsymbol{q}\cdot\boldsymbol{n}_F)^2)}{2}\right) \tag{13}$$

$$F_H(\boldsymbol{q}) = N_H \times \mathrm{sinc}\left(\frac{(\boldsymbol{q}\cdot\boldsymbol{n}_H)L_H}{2}\right) \times \exp\left(\frac{-\sigma_l^2(\boldsymbol{q}\cdot\boldsymbol{n}_H)^2}{2}\right) \times \exp\left(\frac{-\sigma_{Hr}^2(|\boldsymbol{q}|^2 - (\boldsymbol{q}\cdot\boldsymbol{n}_H)^2)}{2}\right) \tag{14}$$

The form factor of the mesogen is just the combination of that of the segments. By definition we can choose the plane of the smectic layer to pass through the junction of the fluorinated and hydrogenated segments. If the fluorinated segment lies below $z = 0$ and the hydrogenated segment above it, the form factor for the entire mesogen is given by

$$F(\boldsymbol{q}) = F_F(\boldsymbol{q}) \exp\left(\frac{-i(\boldsymbol{q}\cdot\boldsymbol{n}_F)L_F}{2}\right) + F_H(\boldsymbol{q}) \exp\left(\frac{i(\boldsymbol{q}\cdot\boldsymbol{n}_H)L_H}{2}\right) \tag{15}$$

where the phase factors arise because the center of each mesogen segment is displaced by a vector

$$\frac{L}{2}\boldsymbol{n}$$

from their junction.

In addition to the form factor, eq 8 also requires the reciprocal lattice vectors $\boldsymbol{q}^j$. If the mesogens are directed along the smectic layer normal, the packing in the $x-y$ plane is pure hexagonal and all six lattice vectors will be of magnitude

$$|\boldsymbol{q}^j| = \frac{2\pi}{D} \times \frac{2}{\sqrt{3}}$$

When the mesogens are tilted over, the hexagonal lattice stretches in the direction of tilt. When the rod director tilts in the $x-z$ plane, the reciprocal lattice vectors distort to

$$\boldsymbol{q}_j = \frac{2\pi}{D} \times \frac{2}{\sqrt{3}} \times \left[-\cos\tau \sin\left(\psi + \frac{j\pi}{3}\right)\hat{\boldsymbol{x}} + \cos\left(\psi + \frac{j\pi}{3}\right)\hat{\boldsymbol{y}}\right] \tag{16}$$

where τ is the tilt angle of the mesogen, ψ the angle from the plane of tilt to the nearest neighbor taken about the tilt axis, and j runs from 1 to 6 giving all six reciprocal lattice vectors. The effect of tilt is to shrink the reciprocal lattice in the direction of tilt. The variable, ψ, relates the direction of tilt to the lattice. For $\psi = 0°$ the tilt is toward a nearest neighbor (smectic I), for $\psi = 30°$ the tilt is between nearest neighbors (smectic F) and the random tilt direction of the smectic C phase can be approximated by averaging $I(\phi)$ for lattices with values of ψ between 0° and 30°.

A more realistic model would also average over a distribution of tilt angles. In practice, all that is required is to compute $I(\phi)$ for a set of values of ψ and τ and sum up the results, weighted by $f(\tau)$. The results of such a fit for the full mesogen are shown in Figure 6b. The distribution function has a mean tilt of $\tau_{COM} = 40.3°$ with $\Delta\tau_{fwhm} \pm 9.6°$. The fit is consistent with the simpler model of Leadbetter and Norris, and the reduction in fwhm is as expected.

In the above calculations, the fluorinated and hydrogenated segments have been treated as a single, rigid rod. However, the hydrogenated portion of the mesogen is considerably more flexible and it is thus reasonable to consider it as a coil rather than the perfect cylinder shown in Figure 8. Without such positional correlations, the small electron density of the hydrogenated segment is dominated by the fluorinated segment. To confirm if models in which the hydrogenated segment have more rotamers along its length are consistent with the measured scattering, one can repeat the calculation using just the form factor of the fluorinated segment. Figure 6b shows this model also fits well with a mean tilt of $\tau_{COM} = 41.2°$ and $\Delta\tau_{fwhm} = \pm 6.7°$.

Acknowledgment. CHESS is a national user facility supported by the National Science Foundation and the National Institutes of Health/National Institute of General Medical Sciences under Award DMR-0225180 and the X-ray laboratory supported by DOE Grant DEFG02-97ER62443. We would also like to acknowledge the Office of Naval Research and the National Science Foundation Division of Materials Research for support of this work through Grants N00014-02-1-0170 and DMR-0208825, respectively. The research made use of the Hudson Mesoscale Processing, Polymer Characterization and Surface Imaging facilities of the Cornell Center for Materials Research (CCMR) with support from the National Science Foundation Materials Research Science and Engineering Centers (MRSEC) program DMR-0079992. C.K.O. would also like to acknowledge his long-standing collaboration and discussions

with Ed Kramer (UCSB) and his group in the study of fluorinated block copolymers.

References and Notes

(1) Bunn, C. W.; Howells, E. R. *Nature* **1954**, *174*, 549.
(2) Jason, R. P.; Dam, R. M. V.; Schorzman, D. A.; Quake, S. R.; DeSimone, J. M. *J. Am. Chem. Soc.* **2004**, *126*, 2322.
(3) Mate, C. M.; Wu, J. *ACS Symp. Series* **2000**, *741*, 405.
(4) Youngblood, J. P.; Andruzzi, L.; Ober, C. K.; Hexemer, A.; Kramer, E. J.; Callow, J. A.; Finlay, J. A.; Callow, M. E. *Biofouling* **2003**, *19*, 91.
(5) Krishnan, S.; Wang, N.; Ober, C. K.; Finlay, J. A.; Callow, M. E.; Callow, J. A.; Hexemer, A.; Sohn, K. E.; Kramer, E. J.; Fischer, D. A. *Biomacromolecules* **2006**, *7*, 1449.
(6) Krishnan, S.; Kwark, Y.-J.; Ober, C. K. *Chem. Record* **2004**, *4*, 315.
(7) Hayakawa, T.; Wang, J.; Xiang, M.; Li, X.; Ueda, M.; Ober, C. K.; Genzer, J.; Sivaniah, E.; Kramer, E. J.; Fischer, D. A. *Macromolecules* **2000**, *33*, 8012.
(8) Genzer, J.; Sivaniah, E.; Kramer, E. J.; Wang, J.; Körner, H.; Xiang, M.; Char, K.; Ober, C. K.; DeKoven, B. M.; Bubeck, R. A.; Chaudhury, M. K.; Sambasivan, S.; Fischer, D. A. *Macromolecules* **2000**, *33*, 1882.
(9) Krishnan, S.; Ober, C. K.; Ramakrishnan, A.; Lin, Q.; Paik, M.; Hexemer, A.; Kramer, E. J.; Fischer, D. *Polym. Prepr. (Am. Chem. Soc., Div. Polym. Chem.)* **2005**, *46*, 613.
(10) Barriet, D.; Lee, T. R. *Curr. Opin. Colloid Interface Sci.* **2003**, *8*, 236.
(11) Mourran, A.; Tartsch, B.; Gallyamov, M.; Magonov, S.; Lambreva, D.; Ostrovskii, B. I.; Dolbnya, I. P.; de Jeu, W. H.; Moeller, M. *Langmuir* **2005**, *21*, 2308.
(12) Al-Hussein, M.; Serero, Y.; Konovalov, O.; Mourran, A.; Möller, M.; de Jeu, W. H. *Macromolecules* **2005**, *38*, 9610.
(13) Ober, C. K.; Wang, J.; Mao, G.; Kramer, E. J.; Chen, J. T.; Thomas, E. L. *Macromol. Symp.* **1997**, *117*, 141.
(14) Wang, J.; Mao, G.; Ober, C. K.; Kramer, E. J. *Macromlecules* **1997**, *30*, 1906.
(15) Kier, L. B.; Hall, L. H. *Molecular Connectivity in Chemistry and Drug Research*; Academic Press: New York, 1976.
(16) Smilgies, D.-M.; Busch, P.; Papadakis, C. M.; Posselt, D. *Synchr. Radiat. News* **2002**, *15*, 35.
(17) Thiel, D. J.; Walter, R. L.; Ealick, S. E.; Bilderback, D. H.; Tate, M. W.; Gruner, S. M.; Eickenberry, E. F. *Rev. Sci. Instrum.* **1995**, *66*, 1477.
(18) Barna, S. L.; Tate, M. W.; Gruner, S. M.; Eickenberry, E. F. *Rev. Sci. Instrum.* **1999**, *70*, 2927.
(19) Busch, P.; Rauscher, M.; Posselt, D.; Smilgies, D.-M.; Papadakis, C. M. *J. Appl. Crystallogr.* **2006**, *39*, 433.
(20) Urushihara, Y.; Nishino, T. *Langmuir* **2005**, *21*, 2614.
(21) Als-Nielsen, J.; Jacquemain, D.; Kjaer, K.; Leveiller, F.; Lahav, M.; Leiserowitz, L. *Phys. Rep.* **1994**, *246*, 251.
(22) Tolan, M. *X-ray Scattering from Soft-Matter Thin Films*; Springer-Verlag: Berlin and Heidelberg, Germany, 1999.
(23) Kjaer, K. *Physica B* **1994**, *198*, 100.
(24) Kaganer, V. M.; Möhwald, H.; Dutta, P. *Rev. Mod. Phys.* **1999**, *71*, 779.
(25) Leadbetter, A. J.; Norris, E. K. *Mol. Phys.* **1979**, *38*, 669.
(26) Als-Nielsen, J.; Kjaer, K. In *Phase Transitions in Soft Condensed Matter*; Riste, T., Sherrington, D., Eds.; Plenum Press: New York, 1989; p 112.
(27) Nostro, P. L.; Chen, S.-H. *J. Phys. Chem.* **1993**, *97*, 6535.
(28) Russell, T. P.; Rabolt, J. F.; Twieg, R. J.; Siemens, R. L.; Farmer, B. L. *Macromolecules* **1986**, *19*, 1135.
(29) Lee, B.; Park, I.; Yoon, J.; Park, S.; Kim, J.; Kim, K.-W.; Chang, T.; Ree, M. *Macromolecules* **2005**, *38*, 4311.
(30) Xu, T.; Zvelindovsky, A. V.; Sevink, G. J. A.; Gang, O.; Ocko, B.; Zhu, Y.; Gido, S. P.; Russell, T. P. *Macromolecules* **2004**, *37*, 6980.
(31) Li, M.; Douki, K.; Goto, K.; Li, X.; Coenjarts, C.; Smilgies, D.-M.; Ober, C. K. *Chem. Mater.* **2004**, *16*, 3800.
(32) Kaganer, V. M.; Peterson, I. R.; Kenn, R. M.; Shih, M. C.; Durbin, M.; Dutta, P. *J. Chem. Phys.* **1995**, *102*, 9412.
(33) Spaar, A.; Salditt, T. *Biophys. J.* **2003**, *85*, 1576.
(34) de Jeu, W. H.; Ostrovskii, B. I.; Shalaginov, A. N. *Rev. Mod. Phys.* **2003**, *75*, 181.
(35) Marczuk, P.; Lang, P. *Macromolecules* **1998**, *31*, 9013.
(36) Bouznik, V. M.; Kirik, S. D.; Solovyov, L. A.; Tzvetnikov, A. K. *Powder Diffraction* **2004**, *19*, 219.

MA061009+